HHS Public Access

Author manuscript

Mol Cancer Res. Author manuscript; available in PMC 2024 September 01.

Published in final edited form as:

Mol Cancer Res. 2024 March 01; 22(3): 308–321. doi:10.1158/1541-7786.MCR-22-0572.

Single-Cell RNA-Seq Analysis of Patient Myeloid-Derived Suppressor Cells and the Response to Inhibition of Bruton's Tyrosine Kinase

Himanshu Savardekar[1,2], **Carter Allen**[2,6], **Hyeongseon Jeon**[6,7], **Jianying Li**[7], **Dionisia Quiroga**[1,5,7], **Emily Schwarz**[1,2], **Richard C. Wu**[1,5], **Sara Zelinskas**[1], **Gabriella Lapurga**[1], **Alexander Abreo**[1], **Andrew Stiff**[1,5], **Jami Shaffer**[1,4], **Bradley W. Blaser**[1,4], **Matthew Old**[3], **Robert Wesolowski**[5], **Gang Xin**[7], **Kari L. Kendra**[1,5], **Dongjun Chung**[6,7], **William E. Carson III**[1,3]

[1]Comprehensive Cancer Center, The Ohio State University, Columbus, Ohio

[2]Biomedical Sciences Graduate Program, The Ohio State University, Columbus, Ohio

[3]Division of Surgical Oncology, Department of Surgery, The Ohio State University, Columbus, Ohio

[4]Division of Hematology, Department of Internal Medicine, The Ohio State University, Columbus, Ohio

[5]Division of Medical Oncology, Department of Internal Medicine, The Ohio State University, Columbus, Ohio

[6]Department of Biomedical Informatics, The Ohio State University, Columbus, Ohio

[7]Pelotonia Institute for Immuno-Oncology, The James Comprehensive Cancer Center, The Ohio State University, Columbus, Ohio

Abstract

Myeloid-derived suppressor cell (MDSC) levels are elevated in cancer patients and contribute to reduced efficacy of immune checkpoint therapy. MDSC express Bruton's Tyrosine Kinase (BTK) and BTK inhibition with ibrutinib, an FDA-approved irreversible inhibitor of BTK, leads to reduced MDSC expansion/function in mice and significantly improves the anti-tumor activity of anti-PD-1 antibody treatments.

Single-cell RNA sequencing (scRNA-seq) was used to characterize the effect of ibrutinib on gene expression of fluorescence activated cell sorting-enriched MDSC from patients with different cancer types (breast, melanoma, head and neck squamous cell cancer - HNSCC). Melanoma patient MDSC were treated*in vitro*for 4h with 5μM ibrutinib or DMSO, processed for scRNA-seq using the Chromium 10x Genomics platform, and analyzed via the Seurat v4 standard integrative workflow.

Corresponding author: William E. Carson III, MD, Division of Surgical Oncology, The Ohio State University, N924 Doan Hall, 410 W. 10th Ave., Columbus, OH 43210, Phone: (614) 293-6306, Fax: (614) 293-3465, william.carson@osumc.edu.

The authors declare no potential conflicts of interest.

Baseline gene expression of MDSC from breast, melanoma, and HNSCC cancerpatientsrevealed similarities among the top expressed genes. *In vitro*ibrutinib treatment of MDSC from melanoma patients resulted in significant changes in gene expression. *GBP1,IL-1β and CXCL8* were among the top downregulated genes while *RGS2* and *ABHD5* were among the top upregulated genes ($p<0.001$). Double positive $CD14^+CD15^+$ MDSC and PMN-MDSC responded similarly to BTK inhibition and exhibited more pronounced gene changes compared to early MDSC and M-MDSC. Pathway analysis revealed significantly downregulated pathwaysincluding TREM1, nitric oxide signaling, and IL-6 signaling ($p<0.004$).

Implications: ScRNA-seq revealedcharacteristic gene expression patternsfor MDSC from different cancer patients and BTK inhibition led to the downregulation of multiple genes and pathways important to MDSC function and migration.

Keywords

Single cell RNA sequencing; scRNA-seq; MDSC; cancer; BTK; ibrutinib; immunotherapy

Introduction

Myeloid-derived suppressor cells (MDSC) are immature myeloid cells that have immunosuppressive properties[1]. In humans, this cell population can be characterized as $CD33^+$, $CD11b^+$ and HLA-$DR^{lo/-}$[2,3]. It has been shown that the MDSC population is abnormally expanded in the setting of cancer and that MDSC localize to tumors and lymphoid tissues. Here, their inhibitory actions on T cells and NK cells lead to the impairment of anti-tumor immune responses[4,5]. MDSC promote immune suppression by multiple methods including the production of arginase-1, indolamine 2, 3-dioxygenase (IDO), nitric oxide (NO), reactive oxygen species (ROS), and inhibitory cytokines (e.g. IL-10,TGF-β)[5]. MDSC also appear to contribute to the expansion of regulatory T lymphocytes[2,5]. The frequency of circulating MDSC has been shown to correlate with tumor burden and has prognostic value in a variety of cancers[6–9]. Studies in murine tumor models have revealed that interventions to reduce MDSC levels or inhibit their function results in improved anti-tumor immune responses and reduced tumor growth[3].

Bruton's tyrosine kinase (BTK) is a B cell receptor pathway kinase that is uniformly overexpressed at the transcript level and constitutively phosphorylated in chronic lymphocytic leukemia (CLL)[10]. Ibrutinib is an FDA-approved, orally administered irreversible BTK inhibitor that is in clinical use for CLL and other B-cell malignancies. Ibrutinib functions by covalently binding to cysteine-481 residue (Cys-481) directly outside of the ATP binding pocket of BTK[10–13]. Previous literature has shown that targeting BTK in malignant B cells with ibrutinib inhibits Bcell receptor signaling via reduced activation of ERK and PLCγ2 with concurrent inhibition of NF-κB signal transduction[14]. Our group has demonstrated that MDSC express Bruton's tyrosine kinase (BTK) and that ibrutinib inhibits MDSC induction, function, and migration to tumors[11]. We have also shown that ibrutinib diminishes MDSC production of nitric oxide (NO), a key mediator responsible for dampening both the innate and antigen specific immune response to cancer[4,11,15]. This effect involves the reaction of NO with superoxide to produce peroxynitrite and the

subsequent tyrosine nitration of key signaling molecules in T cells and NK cells[4]. These studies led to the discovery that ibrutinib significantly enhances the therapeutic efficacy of PD-L1 checkpoint blockade in murine models of cancer[11].

It was hypothesized that an analysis of the effect of ibrutinib on MDSC gene expression could provide additional insight on the genes and pathways that regulate their immunosuppressive functions. Single cell RNA sequencing (scRNA-seq) can provide a window into the transcriptome of specific immune cell populations following targeted perturbations that cannot be achieved via bulk sequencing approaches. For these reasons, scRNA-seq was used to further characterize gene expression in MDSC from human patients with cancer and determine the effects of BTK inhibition with ibrutinib.

Materials and Methods

Patient population and sample procurement

Whole blood was collected from one patient with stage IV head & neck squamous cell carcinoma, one patient with stage IV breast cancer, and three patients with advanced melanoma (one with stage IIID, one with stage IIIA, and one with metastatic stage IV disease). All samples were procured following patient signing of written informed consent conducted in accordance with recognized ethical guidelines under IRB approved protocols for human subject research (IRB protocols 199C0348, 2004C0096, and 2010C0036). Approximately 30 mL of peripheral venous blood was collected from each patient. Peripheral blood mononuclear cells (PBMC) were isolated from peripheral venous blood via density gradient centrifugation with Ficoll, as previously described[16]. Briefly, samples were layered carefully on top of the Ficoll density gradient (density = 1.077 g/mL) medium and centrifuged for 25 minutes at 1500 rpm with the brake off. Using this isolation method, PMN-MDSC remain in the PBMC fraction while PMN are pelleted out over FICOLL. Enriched cell populations were removed from the density gradient medium (plasma interface) and residual red blood cells were lysed. PBMC were used immediately in the experiments described below.

MDSC fluorescence activated cell sorting (FACS) isolation and ibrutinib treatment of MDSC

PBMC at a concentration of 10 million cells per 1 mL of flow cytometry buffer (PBS + 10% FBS) were stained for MDSC markers using fluorescent antibodies at a concentration of 1 μL per 1 million cells for 30 minutes at 4°C. The fluorescent antibodies used for MDSC staining were PE anti-CD11b (Biolegend, #301306), APC anti-CD33 (Biolegend, #366606), PeCy7 anti-HLA-DR (Biolegend, #307616). Stained PBMC were washed twice with 1 mL of PBS and resuspended in sorting buffer (PBS containing 1 mM EDTA) at a concentration of 5 million cells per 1 mL. MDSC isolation was performed via fluorescence-activated cell sorting (FACS) based on ($CD11b^{+}$/ $CD33^{+}$/$HLA\text{-}Dr^{lo/-}$) expression on the BD ARIA 3 (BD Biosciences). Fluorescence minus one (FMO) controls were used for gating. The MDSC purity of samples averaged 75% with >85% viability as measured by post-sort Trypan Blue dye exclusion. 1million freshly purified MDSC from melanoma patients were treated *in vitro* with ibrutinib (5 μM) or (<0.01%) DMSO in 1 mL HAB media (complete RPMI with human AB serum) at 37°C for 4hours and RNA was processed using the Chromium 10X

genomic platform[11]. MDSC viability after 4h remained >80% as measured by Trypan Blue dye exclusion. Reagent information can be found in Supplementary Table 1.

Single cell RNA sequencing and analysis

Freshly enriched MDSC with a cell viability >80% were loaded onto a 10X chip. cDNA was synthesized and amplified, and sequencing libraries were prepared using the 10X Chromium Next GEM 3' gene expression kit (10X Genomics) targeting recovery of 4000 cells per sample[17]. Gene expression libraries were constructed and sequenced according to the manufacturer's instructions (Illumina NovaSeq, Nationwide Children's Hospital Institute for Genomic Medicine/Genomic Services Laboratory). Sequence data were processed using Cell Ranger v3.1.0 for read alignment (against the reference genome GRCh38), transcript reconstruction/annotation, abundance quantification, and read quality trimming. Cell recovery was 3374 (+/− 1154) cells per sample. Seven samples were analyzed via scRNA-seq. All data analyses were performed using R version 4.0.2[18]. Cells with less than 500 genes expressed in each sample were discarded to eliminate low quality and dying cells. Similarly, gene features that were detected in less than 5 cells were discarded. Gene expression was normalized using the LogNormalize approach (function 'NormalizeData') and the 2000 most variable features were extracted for each sample individually (function 'FindVariableFeatures' with selection.method = 'vst') using the standard workflow implemented in the R package Seurat version 4[19]. All samples were integrated as described by Stuart and Butler *et al.*[20]. Specifically, this integrative analysis workflow first identifies cross-dataset pairs of cells that are in a matched biological state ('anchors'; function 'FindIntegrationAnchors') and uses them to correct for technical differences between datasets (i.e., batch effect correction), and to perform comparative scRNA-seq analysis across experimental conditions (function 'IntegrateData'). To facilitate visualization, using the 30 principal components (PCs) (function 'RunPCA'), the high dimensional gene expression features were subjected to dimension reduction using the Uniform Manifold Approximation and Projection (UMAP) algorithm[21] (function 'RunUMAP'). The cells were then clustered using the Louvain algorithm[22] with resolution of 0.5 (function 'FindClusters') and clusters were annotated with cell types using SingleR and PanglaoDB[23]. The Wilcoxon Rank Sum test was used for differential expression (DE) analyses and all DE p-values were adjusted for multiple comparisons using the Bonferroni correction (functions 'FindConservedMarkers' and 'FindMarkers').

Gene expression pathway analysis

Differentially expressed (DE) genes from the MDSC cluster (control vs. ibrutinib, adjusted p-value <0.01) were analyzed via Qiagen Ingenuity Pathway Analysis, RRID:SCR_008653 (IPA). Directionality of canonical pathways affected via regulated genes were displayed as Z scores[17]. IPA selection of genes involved in migration and activation of myeloid cells were compared.

Cell-cell interaction analysis

To comprehensively analyze cell-cell interactions between MDSC and other immune cells, CellChat (v1.4.0) was used[18]. MDSC interaction with the $CD8^+$ T cells, $CD4^+$ T cells, natural killer (NK) cells, and dendritic cells (DC) was evaluated. Potential ligand-receptor

interactions were derived based on the expression of a receptor by one cellsubpopulation and ligand expression by another.

Real time polymerase chain reaction (RT-PCR)

Freshly isolated melanoma MDSC were plated at a concentration of 1 million cells per mL of HAB media in a 24-well plate. DMSO (control) or 1 μM ibrutinib was added for 6h. Viability of MDSC remained >80% as measured by Trypan Blue dye exclusion. RNA was isolated from MDSC using the MirVana miRNA isolation kit. Reverse transcription reactions were performed using 500 ng RNA in a 20μl reaction with the high-capacity reverse transcription kit (Life Technologies). cDNA was used as a template to measure the expression of *GBP1*,*CXCL8*,*CXCL10*,*IL-1*β by quantitative-Real Time PCR using pre-designed primers (Integrated DNA Technologies, Coralville, IA). Human *β-Actin* served as an internal control for each reaction (Integrated DNA Technologies, Coralville, IA). RT-PCR reactions were performed using the ABI PRISM 7900HT fast RT-PCR system with SYBR Green chemistry (Applied Biosystems).[11] Fold changes were calculated using the $2^{-\Delta\Delta Ct}$ method and statistical differences between treatment groups were determined via paired student's t-test[11]. Reagent information can be found in Supplementary Table 1.

Measurement of CXCL8 in supernatants

Freshly isolated melanoma MDSC were plated a concentration of 1 million cells per 1 mL of HAB media in a 24-well plate. DMSO (control), or ibrutinib (1 or 5 μM) was added for 24h. Viability of MDSC remained >80% as measured by SYTOX™ Blue staining. MDSC supernatants were harvested and the concentration of CXCL8 was measured using the Human IL-8/CXCL8 Quantikine ELISA Kit (R&D, #D8000C). Reagent information can be found in Supplementary Table 1

Measurement of adhesion moleclues by flow cytometry

PBMC isolated from melanoma patients were stained with MDSC markers: FITC anti-CD11b (Biolegend, #101206), APC anti-CD33 (Biolegend, #366606), PeCy7 anti-HLA-DR (Biolegend, #307616) and isolated via fluorescence-activated cell sorting (FACS) based on ($CD11b^{+}$/ $CD33^{+}$/$HLA\text{-}Dr^{lo/-}$) expression. MDSC were then were plated a concentration of 1million cells per mL of HAB media in a 24-well plate. DMSO (control), or ibrutinib (1 or 5 μM) was added for 24h. MDSC were then trypsinized and collected, washed twice with PBS, and stained in flow cytometry buffer with either PE anti-ICAM-1 (Biolegend, #353105) or PE anti-ALCAM (Biolegend, #343903). Staining was performed for 30 minutes at 4°C. MDSC were then washed twice with flow cytometry buffer and expression of ICAM-1 and ALCAM was measued on the BD Fortessa. Fluoresence minus one controls were used for gating the PE positive populations. Reagent information can be found in Supplementary Table 1.

Statistical analysis

The Wilcoxon Rank Sum test was used for differential expression (DE) analyses. All DE p-values were adjusted for multiple comparisons using the Bonferroni correction. For RT-PCR

and protein analysis, statistical differences between treatment groups were determined via paired student's t-tests.

Data Availability

The data generated in this study are publicly available in Gene Expression Omnibus (GEO) atGSE210963.

Results

Cell groupings identified by single cell RNA-seq analysis of cancer PBMC enriched for MDSC.

PBMC were isolated from the whole blood of five cancer patients (3 with melanoma, 1 head & neck, and 1 breast) and enriched for MDSC ($CD11b^+$, $CD33^+$, HLA-$DR^{lo/-}$) using FACS. Patient characteristics are provided in Supplementary Table 2. MDSC purity was 75% on average (Supplementary Figure S1). MDSC samples were processed for mRNA and evaluated via scRNA-seq as described above. Clusters annotated by SingleR[19] were used to identify the major immune cell populations present in the baseline samples following enrichment (Figure 1A). The Louvain clustering algorithm identified 7 distinct cell clusters based on canonical cell markers[8]. MDSC comprised the majority of cells. $CD4^+$ T cells, $CD8^+$ T cells, dendritic cells, eosinophils, basophils, and natural killer (NK) cells represented the minor cell populations that remained after MDSC enrichment (Figure 1B). The validity of the annotated cell clusters was confirmed by an analysis of gene expression in each cell population using the Panglao database[20] (Figure 1C and Supplementary Figure S2). As expected, the MDSC population represented the majority of the cells in this analysis.

Gene expression of MDSC expression from patients with different cancer types.

Baseline gene expression from breast, head & neck, and melanoma cancer patients revealed a similar pattern of highly expressed genes in the MDSC cluster compared to all other cell populations present in the sample. **Tables 1, 2, and 3** list the top DE expressed genes in the MDSC cluster for each cancer type where there was at least a 2.5 $\log_2$-fold increase in expression relative to the other cell populations. This approach led to the identification of 14 DE genes in head & neck cancer MDSC, 13 DE genes in breast cancer MDSC, and 8 DE genes in melanoma MDSC. The top 4 upregulated genes in these three samples were *S100A8*, *S100A9*, *VCAN* (versican), and *LYZ* (lysozyme)[21]. *MNDA* (myeloid cell nuclear cell differentiation antigen) and *CD14* were also upregulated in all MDSC samples. *CYBB* had a 2.4 $\log_2$-fold increase in head & neck MDSC, a 1.5 $\log_2$-fold increase in breast MDSC, and a 1.1 $\log_2$-fold increase in melanoma MDSC. *CD36* showed a 2.3 $\log_2$-fold increase in head & neck MDSC, a 2.8 $\log_2$-fold increase in breast MDSC, and a 0.9 $\log_2$-fold increase in melanoma MDSC (Supplementary Table 4).[22] UMAP plots of *S100A8*, *CYBB*, *CD36*, and *VCAN* expression demonstrate that these genes were selectively expressed in the MDSC cluster (Figure 2A). An exploratory comparison of MDSC gene expression was conducted between individual cancer patients to highlight the effect of inter-patient variables (age, sex race, cancer type) on overall gene regulation. It is important to note that no conclusions can made as to the effect of tumor histology on MDSC gene expression given the presence of other variables. Given the small sample sizes,

these comparisons must be viewed as case studies that can serve as a basis for future, larger studies of homogenous patient populations. As expected, these confounding factors did impact the MDSC gene expression pattern to a significant degree. An analysis of the variability of MDSC gene expression between a head & neck cancer patient and a breast cancer patient is provided as a volcano plot in Figure 2B. MDSC genes upregulated in the head & neck cancer patient compared to that of a highly dissimilar breast cancer patient are highlighted in red. The top upregulated MDSC genes in a head & neck cancer patient compared to a breast cancer patient include *RPS4Y1* and *CD52*. MDSC genes upregulated in a breast cancer patient compared to a head & neck cancer patient are highlighted in blue. The top upregulated MDSC genes in this individual breast cancer patient compared to the head & neck cancer patient include *MTRNR2L12*, *XIST,* and *EGR2*. The top ten upregulated genes in these individual samples are listed in the adjacent table. Importantly, these differences in gene expression could be related to any one of a number of factors given the multiple variables that are out of alignment between these two patients. An additional comparison of MDSC gene expression between a melanoma patient and the two other cancer patients (breast and head & neck) is shown in Supplementary Figure S3 and confirms the impact of patient variables on MDSC gene expression. For example, *HIF1A* (hypoxia inducing factor 1) was upregulated 3.5 $\log_2$-fold in MDSC from a melanoma patient compared to MDSC from a breast cancer patient and 3.8 $\log_2$-fold when compared to MDSC from a patient with head and neck cancer. *MNDA* was found to be more highly expressed in MDSC from breast (2.6 $\log_2$-fold) and head & neck (3.0 $\log_2$-fold) cancer patients compared to a melanoma patient. These differences in MDSC gene expression across different patients with different cancers highlights the importance of inter-patient variability in MDSC gene analysis and indicate the need for additional studies that evaluate patients that are highly similar in all respects. Given the many differences between the patients being studied here, it is not currently possible to make definitive conclusions from the above analyses.

Changes in gene expression following *in vitro* treatment of MDSC from melanoma patients with ibrutinib.

Our group has previously demonstrated that BTK inhibition with ibrutinib exerts an inhibitory effect on MDSC function[11]. Therefore, scRNA-seq was used to evaluate the effect of ibrutinib on gene expression in MDSC isolated from two melanoma patients. Patient MDSC were treated for 4hours with 5 μM ibrutinib or DMSO control. The Louvain clustering algorithm identified 7 distinct cell populations which did not shift significantly following short term treatment with ibrutinib (Figure 3A and Supplementary Figure S4). DE genes in the MDSC cluster following BTK inhibition are displayed as a volcano plot with the top down-regulated genes highlighted in red and the top upregulated genes shown in blue (Figure 3B). **Table 3C** lists the top DE genes in the MDSC cluster that exhibited at least a 0.5 $\log_2$-fold change in expression relative to DMSO control with a p-value <0.001. This approach led to the identification of 26 downregulated genes and 4 upregulated genes. *GBP1*, *IRF1*, *CXCL10*, and *IL-1β* exhibited markedly reduced expression, while *RGS2*, *ZFP36L2*, *LYZ*, and *ABHD5* demonstrated increased expression. Notably, these genes have been previously implicated in MDSC function.[23,24]

MDSC gene expression pathway analysis following BTK inhibition.

Further examination of gene expression patterns following BTK inhibition were conducted using Ingenuity Pathway Analysis (IPA). This analysis was performed based on the DE genes in the MDSC cluster (highest $\log_2$-fold change for control vs. ibrutinib, $p<0.01$) and displays upregulated pathways with a positive z-score and downregulated pathways with a negative z-score (Figure 4A). This assessment revealed that multiple pathways important to MDSC function were downregulated following inhibition of BTK. The TREM1 signaling pathway was downregulated with a z-score of −3.0 (Supplementary Figure S5). This pathway has been shown to be involved in the secretion of proinflammatory cytokines by MDSC and tumor-associated macrophages. Futhermore, TREM1 upregulation in MDSC is associated with progression of several mouse and human cancers[25]. The NFR2 oxidative stress response pathway was also downregulated with a −2.3 z-score. This pathway is important for MDSC survival in the presence of reactive oxygen species[26]. Nitric oxide signaling is important for MDSC suppression of T cell activity and was downregulated with z-score of −1.27[11]. The IL-6 and IL-8 signaling pathways were downregulated with a z-score of −2.1 and −1.3, respectively[27]. Finally, TLR (Toll-like receptor) signaling was downregulated with a z-score of −1.6[28]. In contrast, the peroxisome proliferator-activated receptor (PPAR) signaling pathway was upregulated with a z-score of 2.6 after ibrutinib treatment. PPAR signaling via lysosomal acid lipase has been shown to be critical for MDSC accumulation and ROS production[29]. The genes belonging to TREM1, NRF-2 pathway, nitric oxide production, IL-6 and 8, and PPAR pathways are displayed in Figure 4B. A number of genes such as *IL-1β* and *CXCL8* participate in more than one of the pathways listed above. Ibrutinib also downregulated multiple genes associated with functions of cellular movement and macrophage activation as shown in Figure 4C.

Communication of MDSC with other cell types via ligand-receptor interactions.

The communication between cell clusters (MDSC, $CD8^+$ T cells, $CD4^+$ T cells, NK cells, and dendritic cells) was evaluated via ligand-receptor interactions using CellChat (v1.4.0)[18]. These communications represent hypothetical *in silico* interactions in which the gene expression of known ligand-receptor pairs was assessed in each cell cluster from melanoma patient samples. These interactions are displayed in a circle plot where the size of the dot represents the number of cells within each cluster. As expected, MDSC interacted with $CD8^+$ T cells, $CD4^+$ T cells, NK cells, and dendritic cells (Figure 5A). Arrows emanating from the MDSC cluster represent ligands for which there is a corresponding receptor expressed on the target cell type. The thickness of the arrows represents the number of interactions. The MDSC cluster has more interactions with $CD8^+$ T cells compared to $CD4^+$ T cells, NK cells, and dendritic cells. Specific MDSC ligand-receptor interactions with $CD8^+$ T cells, NK cells, and $CD4^+$ T cells in DMSO and ibrutinib treated samples are displayed in Figure 5B. Ibrutinib treatment led to increased antigen presenting *HLA-CD8* interactions between MDSC and $CD8^+$ T cells compared to DMSO control. While these interactions are not known to occur in the periphery, such interactions could occur within the tumor microenvironment.

MDSC subset gene expression after in vitro ibrutinib treatment.

Gene expression changes within MDSC subpopulations after *in vitro* ibrutinib treatment were also examined. These included M-MDSC ($CD14^+$), PMN-MDSC ($CD15^+$), double positive MDSC ($CD14^+$, $CD15^+$), and a double negative population referred to as early MDSC ($CD14^-$, $CD15^-$). CD14 and CD15 gene expression within the MDSC cluster was utilized to identify the MDSC subsets. Expression thresholds to identify the negative and positive populations are shown in Supplmentary Figure S6. The M-MDSC subset accounted for the majority of cells in the MDSC population at 59.9% and PMN-MDSC comprised 2.8% of MDSC. Early MDSC made up 29.4% of the MDSC population, whereas 7.9% of MDSC expressed both CD14 and CD15 (Figure 6A). DE genes for each MDSC subset after ibrutinib treatment are displayed as a volcano plot (Figure 6B). Gene expression changes in each MDSC subset mirrored changes in the total MDSC population. *GBP1*, *IRF1*, *APOL6* were the top significantly downregulated genes among each of the MDSC subsets while *RGS2*, *CEBPD*, *ABHD5* were consistently the top upregulated genes in each subset. Changes in the DE patterns of genes important to MDSC function and accumulation were less pronounced in the early MDSC population compared to the other MDSC subsets (Figure 6C). Of note, *CXCL10* was downregulated −3.7 $\log_2$-fold in double positive MDSC and −3.5 $\log_2$-fold in PMN-MDSC, but less so in M-MDSC (−2.5 $\log_2$-fold) and early MDSC (−1.5 $\log_2$-fold). *GBP1* had expression trends similar to *CXCL10*. *IL-1β* was downregulated similarly in all four MDSC subsets (−1.7 to −2.0 $\log_2$-fold decrease). Among the top upregulated genes in each subset, pro-angiogenic *RGS2* had a similar change expression in double positive MDSC (1.5 $\log_2$-fold), PMN-MDSC (1.3 $\log_2$-fold), and M-MDSC (1.2 $\log_2$-fold) while being less upregulated in double negatives (0.7 $\log_2$-fold). *CXCR4* (linked to MDSC migration and accumulation in tumors) behaved in a similar fashion.[28,30]

Double positive MDSC gene expression analysis.

$CD14^+CD15^+$ MDSC (referred to as “double positives”) have been likened to an activated population of PMN-MDSC[49]. The double positive and $CD15^+$ PMN-MDSC populations were compared via DE analysis. This analysis revealed 6 genes that were significantly upregulated in double positive MDSC compared to PMN-MDSC in head and neck cancer. These genes included *CD14*, *S100A8*, *S100A9*, *S100A12*, *VCAN*, and *METTL9* (Supplementary Figure S7A). Only 2 genes were significantly upregulated in the double positive subset in breast MDSC (*CD14*, *RETN*) when compared to $CD15^+$ MDSC. (Supplementary Figure S7 B). However, double positive MDSC and PMN-MDSC responded similarly to BTK inhibition and exhibited more pronounced gene changes when compared to early MDSC and M-MDSC (Figure 6C).

MDSC PCR and protein analysis of select genes after BTK inhibition.

To confirm gene expression changes in MDSC after BTK inhibition from single cell analysis, purified MDSC from melanoma patients were treated for 6 h with ibrutinib or DMSO control. RNA was isolated from cells in each experimental condition and selected top genes from the single cell data set were analyzed via PCR. *β-actin* was used as a control gene in this analysis. *CXCL10* expression was significantly decreased 59% after ibrutinib

treatment compared to DMSO control ($p<0.01$) (Figure 7A). *IL-1β* expression decreased 66% after ibrutinib treatment compared to DMSO control which was almost statsticially significant ($p=0.08$) (Figure 7B). *GBP1* expression was significantly decreased 44% after ibrutinib treatment compared to DMSO control ($p<0.05$) (Figure 7C). CXCL8 expression was significantly decreased by 68% after ibrutinib treatment compared to DMSO control ($p<0.05$) (Figure 7D). Additionally, BTK inhibition with ibrutinib led to a significant, dose-dependent reduction of CXCL8 secretion by MDSC after 24h with no effect on MDSC viability (Figure 7E and Supplemental Figure S8). Futhermore, expression of adhesion molecules ICAM-1 and ALCAM were found to be significantly reduced on MDSC after ibrutinib treatment as well (Figure 7F and 7G).

Discussion

There are many compelling studies showing the immunosuppressive functions of MDSC and their correlation with poor outcomes in immune-based cancer therapies[5,8]. Targeting MDSC for elimination or deactivation has been linked to better outcomes for cancer patients and a more efficacious response to immunotherapy[5]. The goal of this study was to characterizebaseline gene expression of MDSC from patients with different cancer types using single-cell RNA sequencing and to distinguish the gene expression changes in MDSC after *in vitro* inhibition of BTK with ibrutinib. BTK is an important mediator of MDSC biology as previously shown by our group[11]. In the present study, it was found that MDSC from different cancer types (head & neck, breast, and melanoma) had similar highly expressed genes (*S100A8, S100A9, LYZ, VCAN)* compared to the other cell types present in the sample. These genes have been previously identified as being expressed in MDSC when compared to other cell populations including monocytes[31]. BTK inhibition of MDSC from melanoma patients led to downregulation of several genesand pathways associated with MDSC migration and function. These included genes such as *IL-1β* and *GBP1* and pathways such as the TREM1 signaling pathway and the nitric oxide production pathway. The gene expression of MDSC subsets ($CD15^+$ PMN-MDSC, $CD14^+$ M-MDSC, double negative (early) MDSC, and double positive MDSC) were also compared. Notably, ibrutinib-induced regulation of genes was more pronounced in the PMN-MDSC and the double positive subset. Analysis of cellular communication via ligand-receptor interactions between cell clusters revealed that the HLA-B-CD8α ligand-receptor interaction between MDSC and $CD8^+$ T cells was enriched after ibrutinib treatment. Haile *et al* highlighted a crucial role of antigen presentation by MDSC via MHC-I as a necessary mechanism of suppression of $CD8^+$ T cells[32]. The present study demonstrated that MDSC gene expression and the response to targeted inhibitory treatments can be precisely measured via single-cell sequencing techniques.

Baseline MDSC gene expression from all three cancers (breast, head & neck cancer, and melanoma) aligns with MDSC defining biomarkers. This includes genes encoding calcium binding proteins (*S100A8/A9/A12*) and genes contributing to immune suppression (*CYBB*)[3]. CD36, a fatty acid translocase highly expressed by MDSC from both breast and head & neck cancer patients, has been shown to support MDSC immunosuppression through fatty acid uptake. Inhibition of CD36 in murine tumors was found to reduce the immunosuppressive function of tumor-infiltrating MDSC in a $CD8^+$ T cell-dependent

manner[22]. Versican, an extracellular matrix proteoglycan, is encoded by the gene *VCAN* and was selectively upregulated in MDSC from all three cancer populations. Within the tumor microenvironment, MDSC secretion of versican has been shown to accelerate tumor growth and metastasis in a murine breast cancer model and is associated with lower infiltration of $CD8^+$ T cells in colorectal cancer indicating that versican may restrict T cell infiltration[33–35]. Myeloid cell nuclear differentiation antigen (*MNDA)*, which is associated with neutrophil function, is upregulated in human M-MDSC compared to monocytes in peripheral blood of advanced non-small cell lung cancer patients[36]. *MNDA* was expressed at 3.4 $\log_2$-fold higher levels in head & neck MDSC, 2.7 $\log_2$-fold higher levels in breast MDSC, and 1.0 $\log_2$-fold higher levels in melanoma MDSC compared to the other cell populations (T cells, NK cells, dendritic cells, eosinophils, and basophils). In the context of MDSC biology, these highly expressed genes can all exhibit a pro-tumor effect.

This is the first reported experimental study using single-cell RNA sequencing to analyze gene expression changes in MDSC after *in vitro* BTK inhibition with ibrutinib. BTK inhibition in MDSC resulted in downregulation of several genes associated with migration (*ALCAM*, *ICAM*, *CXCL10*, *CXCL8*). Downregulation of adhesion molecules (ALCAM and ICAM) and the chemokine CXCL8 by ibrutinib were verified at the protein level. Together, these results could explain the ability of BTK inhibition to decrease MDSC migration into tumor tissues and limit MDSC suppressive ability toward Tcells in the tumor microenvironment[11]. Multiple pathways associated with MDSC function were downregulated after ibrutinib treatment. These included the nitric oxide, NRF2 oxidative stress response, TREM1, IL-6, and TLR pathways. All of these pathways have been associated with the immuno-suppressive properties of MDSC[7,20,26,29]. Our group has previously demonstrated the role of nitric oxide secretion by MDSC in the inhibition of NK cell function via inactivation of FcR signal transduction[13]. Inhibition of MDSC iNOS restored NK cell function and signal transduction in that study. The downregulation of the nitric oxide pathway by ibrutinib in MDSC may remove the cells' suppressive actions and restore the function of cytotoxic cells in the tumor microenvironment. NRF2 is a master regulator of anti-oxidative responses which induces expression of antioxidants and cytoprotective genes[37]. Downregulation of the NRF2 response pathway by ibrutinib in MDSC may leave these cells exposed to oxidative stress from reactive oxygen species, leading to MDSC death. TREM1 expression on MDSC has been shown to increase with tumor growth in a murine triple-negative breast cancer model (4T1)[38]. Increased soluble TREM1 has been found in the plasma of renal cell carcinoma patients and correlated with disease stage[38]. TREM1 has also been linked to TNF signaling in MDSC which has been shown to contribute to MDSC function and accumulation[25]. Therefore, targeting the TREM1 pathway in MDSC may limit the immune suppressive functions of MDSC. Overall, the literature supports the importance of these highlighted genes and pathways in MDSC function and the current report emphasizes the ability of BTK inhibition to modulate these genes.

There is growing experience with human MDSC single-cell transcriptomics, and the current data set aligns with other studies which have employed single-cell analysis to determine baseline gene expression of MDSC. In our results, MDSC functional genes (*CYBB*, *S100A8*, and *RETN*) were upregulated in MDSC from patients with breast and head and

neck cancer. This same pattern was identified in MDSC isolated from peripheral blood of patients with sepsis and canines with melanoma[31,39]. However, MDSC from sepsis patients did not express other classical MDSC genes (*IL-1β*, *IL*-6, *IL-8*, *CEBPB*, *STAT3*) identified in this project[31].

The precise role of PMN-MDSC in tumor biology is currently being examined, and one prevalent hypothesis is that PMN-MDSC emerge from an abnormal neutrophil trajectory[36]. In the spleens of mice, PMN-MDSC were found by Veglia *et al* to gradually replace classical neutrophils as tumors progressed[49]. Within the tumors of these mice, three subsets of PMN were identified: PMN-1 which represented classical neutrophils, PMN-MDSC (with expression of induced NO synthase [iNOS] *S100A9*, *sXBPS1*, and *CD36*), and an activated population of PMN-MDSC with CD14+ expression[40]. These murine CD14+ PMN-MDSC could be analogous to the double-positive human MDSC identified in the present study since both expressed high levels of S100A8 and S100A9 as measured by scRNA-seq. When this group compared murine PMN-MDSC to murine $CD14^+$ PMN-MDSC, the latter had higher expression of genes associated with cell activation, inflammation, and ER stress including *CCL4*, *CCL3* and *SOCS*[40]. However, in the present study there were fewer differences in gene expression between human PMN-MDSC and $CD14^+$ PMN-MDSC. The lower tumor burden of the patients in this study as compared to the murine experiment may have contributed to this finding. As expected, *CD14* was significantly upregulated in human $CD14^+$ PMN-MDSC as compared to PMN-MDSC in both breast and head and neck cancer. Genes encoding the S100 family of proteins (*S100A8*, *S100A9*, *S100A12*) and versican (*VCAN*) were significantly overexpressed in human $CD14^+$ PMN-MDSC as compared to PMN-MDSC in head and neck cancer. Secretion of versican may contribute to mesenchymal-epithelial transition (MET) of cancer cells[41]. S100A9 can regulate MDSC-mediated immune suppression via the RAGE and TLR4 signaling pathways in colorectal carcinoma[42]. Notably, human $CD15^+CD14^+$ MDSC and $CD15^+CD14^-$ PMN-MDSC responded similarly to BTK inhibition with ibrutinib. Gene expression profiling of MDSC subsets following targeted therapies may yield additional clues as to their functions in the setting of cancer.

In conclusion, this report demonstrates that the scRNA-seq gene expression patterns of MDSC from different cancer patients are similar, that multiple genes and pathways important to MDSC function and migration are down-regulated following BTK inhibition, and that a comparative analysis of gene expression in MDSC subsets reveals distinct differences. An understanding of gene expression patterns of MDSC may inform the development of MDSC-specific targeted therapies to enhance the efficacy of immune-based treatments for cancer.

Supplementary Material

Refer to Web version on PubMed Central for supplementary material.

Acknowledgments

The authors thank the patients and their families, the investigators, research nurses, study coordinators, and operations staff who contributed to this study. This study was supported by P30 CA016058 (WEC), T32CA90338

(WEC), T32 CA247815 (DQ), and UM1CA186712 (WEC). This work was supported by the Pelotonia Institute of Immuno-oncology (PIIO), Department of Biomedical informatics/BioInformatics Shared Resource, and the Flow Cytometry Shared Resource at The Ohio State University Comprehsneive Cancer Center. Dr. Carson's research is supported by The John B. and Jane T. McCoy Chair in Cancer Research Endowment.

References

1. Lechner MG, Liebertz DJ, Epstein AL. Characterization of Cytokine-Induced Myeloid-Derived Suppressor Cells from Normal Human Peripheral Blood Mononuclear Cells. J Immunol. 2010;185(4). doi:10.4049/jimmunol.1000901
2. Gabrilovich DI, Nagaraj S. Myeloid-derived suppressor cells as regulators of the immune system. Nat Rev Immunol. 2009;9(3). doi:10.1038/nri2506
3. Bronte V, Brandau S, Chen SH, et al. Recommendations for myeloid-derived suppressor cell nomenclature and characterization standards. Nat Commun. 2016;7. doi:10.1038/ncomms12150
4. Markowitz J, Wang J, Vangundy Z, et al. Nitric oxide mediated inhibition of antigen presentation from DCs to CD4+ T cells in cancer and measurement of STAT1 nitration. Sci Rep. 2017;7(1):15424. doi:10.1038/s41598-017-14970-0 [PubMed: 29133913]
5. Wesolowski R, Markowitz J, Carson WE. Myeloid derived suppressor cells - a new therapeutic target in the treatment of cancer. J Immunother Cancer. 2013;1. doi:10.1186/2051-1426-1-10
6. Meyer C, Cagnon L, Costa-Nunes CM, et al. Frequencies of circulating MDSC correlate with clinical outcome of melanoma patients treated with ipilimumab. Cancer Immunol Immunother. 2014;63(3). doi:10.1007/s00262-013-1508-5
7. Markowitz J, Brooks TR, Duggan MC, et al. Patients with pancreatic adenocarcinoma exhibit elevated levels of myeloid-derived suppressor cells upon progression of disease. Cancer Immunol Immunother. 2015;64(2). doi:10.1007/s00262-014-1618-8
8. Wesolowski R, Duggan MC, Stiff A, et al. Circulating myeloid-derived suppressor cells increase in patients undergoing neo-adjuvant chemotherapy for breast cancer. Cancer Immunol Immunother. 2017;66(11). doi:10.1007/s00262-017-2038-3
9. Mundy-Bosse BL, Thornton LM, Yang HC, Andersen BL, Carson WE. Psychological stress is associated with altered levels of myeloid-derived suppressor cells in breast cancer patients. Cell Immunol. 2011;270(1). doi:10.1016/j.cellimm.2011.04.003
10. Good L, Benner B, Carson WE. Bruton's tyrosine kinase: an emerging targeted therapy in myeloid cells within the tumor microenvironment. Cancer Immunol Immunother. Published online 2021. doi:10.1007/s00262-021-02908-5
11. Stiff A, Trikha P, Wesolowski R, et al. Myeloid-Derived Suppressor Cells Express Bruton's Tyrosine Kinase and Can Be Depleted in Tumor-Bearing Hosts by Ibrutinib Treatment. Cancer Res. 2016;76(8):2125–2136. doi:10.1158/0008-5472.CAN-15-1490 [PubMed: 26880800]
12. Sun SH, Benner B, Savardekar H, et al. Effect of Immune Checkpoint Blockade on Myeloid-Derived Suppressor Cell Populations in Patients With Melanoma. Front Immunol. 2021;12:4239. doi:10.3389/fimmu.2021.740890
13. Stiff A, Trikha P, Mundy-Bosse B, et al. Nitric oxide production by myeloid-derived suppressor cells plays a role in impairing Fc receptor–mediated natural killer cell function. Clin Cancer Res. 2018;24(8). doi:10.1158/1078-0432.CCR-17-0691
14. Herman SEM, Mustafa RZ, Gyamfi JA, et al. Ibrutinib inhibits BCR and NF-κB signaling and reduces tumor proliferation in tissue-resident cells of patients with CLL. Blood. 2014;123(21). doi:10.1182/blood-2014-02-548610
15. Mundy-Bosse BL, Lesinski GB, Jaime-Ramirez AC, et al. Myeloid-Derived Suppressor Cell Inhibition of the IFN Response in Tumor-Bearing Mice. Cancer Res. 2011;71(15):5101–5110. doi:10.1158/0008-5472.CAN-10-2670 [PubMed: 21680779]
16. Benner B, Scarberry L, Suarez-Kelly LP, et al. Generation of monocyte-derived tumor-associated macrophages using tumor-conditioned media provides a novel method to study tumor-associated macrophages in vitro. J Immunother Cancer. 2019;7(1):140. doi:10.1186/s40425-019-0622-0 [PubMed: 31138333]
17. Krämer A, Green J, Pollard J, Tugendreich S. Causal analysis approaches in ingenuity pathway analysis. Bioinformatics. 2014;30(4). doi:10.1093/bioinformatics/btt703

18. Jin S, Guerrero-Juarez CF, Zhang L, et al. Inference and analysis of cell-cell communication using CellChat. Nat Commun. 2021;12(1):1088. doi:10.1038/s41467-021-21246-9 [PubMed: 33597522]
19. Aran D, Looney AP, Liu L, et al. Reference-based analysis of lung single-cell sequencing reveals a transitional profibrotic macrophage. Nat Immunol. 2019;20(2). doi:10.1038/s41590-018-0276-y
20. Franzén O, Gan LM, Björkegren JLM. PanglaoDB: A web server for exploration of mouse and human single-cell RNA sequencing data. Database. 2019;2019(1). doi:10.1093/database/baz046
21. Trovato R, Canè S, Petrova V, Sartoris S, Ugel S, De Sanctis F. The Engagement Between MDSCs and Metastases: Partners in Crime. Front Oncol. 2020;10. doi:10.3389/fonc.2020.00165
22. Al-Khami AA, Zheng L, Del Valle L, et al. Exogenous lipid uptake induces metabolic and functional reprogramming of tumor-associated myeloid-derived suppressor cells. Oncoimmunology. 2017;6(10). doi:10.1080/2162402X.2017.1344804
23. Condamine T, Mastio J, Gabrilovich DI. Transcriptional regulation of myeloid-derived suppressor cells. J Leukoc Biol. 2015;98(6). doi:10.1189/jlb.4ri0515-204r
24. Shi H, Zhang J, Han X, et al. Recruited monocytic myeloid-derived suppressor cells promote the arrest of tumor cells in the premetastatic niche through an IL-1β-mediated increase in E-selectin expression. Int J Cancer. 2017;140(6). doi:10.1002/ijc.30538
25. Carla Bosco M, Raggi F, Varesio L. Therapeutic Potential of Targeting TREM-1 in Inflammatory Diseases and Cancer. Curr Pharm Des. 2017;22(41). doi:10.2174/1381612822666160826110539
26. Ohl K, Fragoulis A, Klemm P, et al. Nrf2 is a central regulator of metabolic reprogramming of myeloid-derived suppressor cells in steady state and sepsis. Front Immunol. 2018;9(JUL). doi:10.3389/fimmu.2018.01552
27. Tobin RP, Jordan KR, Kapoor P, et al. IL-6 and IL-8 Are Linked With Myeloid-Derived Suppressor Cell Accumulation and Correlate With Poor Clinical Outcomes in Melanoma Patients. Front Oncol. 2019;9. doi:10.3389/fonc.2019.01223
28. Ray A, Chakraborty K, Ray P. Immunosuppressive MDSCS induced by TLR signaling during infection and role in resolution of inflammation. Front Cell Infect Microbiol. 2013;4(SEP). doi:10.3389/fcimb.2013.00052
29. Zhao T, Du H, Blum JS, Yan C. Critical role of PPARγ in myeloid-derived suppressor cellstimulated cancer cell proliferation and metastasis. Oncotarget. 2016;7(2). doi:10.18632/oncotarget.6414
30. Obermajer N, Muthuswamy R, Odunsi K, Edwards RP, Kalinski P. PGE 2-induced CXCL 12 production and CXCR4 expression controls the accumulation of human MDSCs in ovarian cancer environment. Cancer Res. 2011;71(24). doi:10.1158/0008-5472.CAN-11-2449
31. Darden DB, Bacher R, Brusko MA, et al. Single-Cell RNA-seq of Human Myeloid-Derived Suppressor Cells in Late Sepsis Reveals Multiple Subsets With Unique Transcriptional Responses: A Pilot Study. Shock. 2021;55(5). doi:10.1097/SHK.0000000000001671
32. Haile LA, Greten TF, Korangy F. Immune suppression: the hallmark of myeloid derived suppressor cells. Immunol Invest. 2012;41(6–7):581–594. doi:10.3109/08820139.2012.680635 [PubMed: 23017136]
33. Cha YJ, Koo JS. Role of Tumor-Associated Myeloid Cells in Breast Cancer. Cells. 2020;9(8). doi:10.3390/cells9081785
34. Johnson KA, Emmerich P, Matkowskyj KA, Deming DA. Predicting CD8+ T-cell infiltration in colorectal cancer using versican proteolysis across molecular profiles. J Clin Oncol. 2020;38(4_suppl). doi:10.1200/jco.2020.38.4_suppl.189
35. Wight TN, Kang I, Evanko SP, et al. Versican—A Critical Extracellular Matrix Regulator of Immunity and Inflammation. Front Immunol. 2020;11. doi:10.3389/fimmu.2020.00512
36. Mastio J, Condamine T, Dominguez G, et al. Identification of monocyte-like precursors of granulocytes in cancer as a mechanism for accumulation of PMN-MDSCs. J Exp Med. 2019;216(9). doi:10.1084/jem.20181952
37. Vomund S, Schäfer A, Parnham MJ, Brüne B, Von Knethen A. Nrf2, the master regulator of anti-oxidative responses. Int J Mol Sci. 2017;18(12). doi:10.3390/ijms18122772
38. Ford JW, Gonzalez-Cotto M, MacFarlane AW, et al. Tumor-Infiltrating Myeloid Cells Co-Express TREM1 and TREM2 and Elevated TREM-1 Associates With Disease Progression in Renal Cell Carcinoma. Front Oncol. 2022;11. doi:10.3389/fonc.2021.662723

39. Jackson K, Milner RJ, Doty A, et al. Analysis of canine myeloid-derived suppressor cells (MDSCs) utilizing fluorescence-activated cell sorting, RNA protection mediums to yield quality RNA for single-cell RNA sequencing. Vet Immunol Immunopathol. 2021;231. doi:10.1016/j.vetimm.2020.110144

40. Veglia F, Hashimoto A, Dweep H, et al. Analysis of classical neutrophils and polymorphonuclear myeloid-derived suppressor cells in cancer patients and tumor-bearing mice. J Exp Med. 2021;218(4). doi:10.1084/JEM.20201803

41. Gao D, Joshi N, Choi H, et al. Myeloid progenitor cells in the premetastatic lung promote metastases by inducing mesenchymal to epithelial transition. Cancer Res. 2012;72(6). doi:10.1158/0008-5472.CAN-11-2905

42. Huang M, Wu R, Chen L, et al. S100A9 Regulates MDSCs-Mediated Immune Suppression via the RAGE and TLR4 Signaling Pathways in Colorectal Carcinoma. Front Immunol. 2019;10. doi:10.3389/fimmu.2019.02243

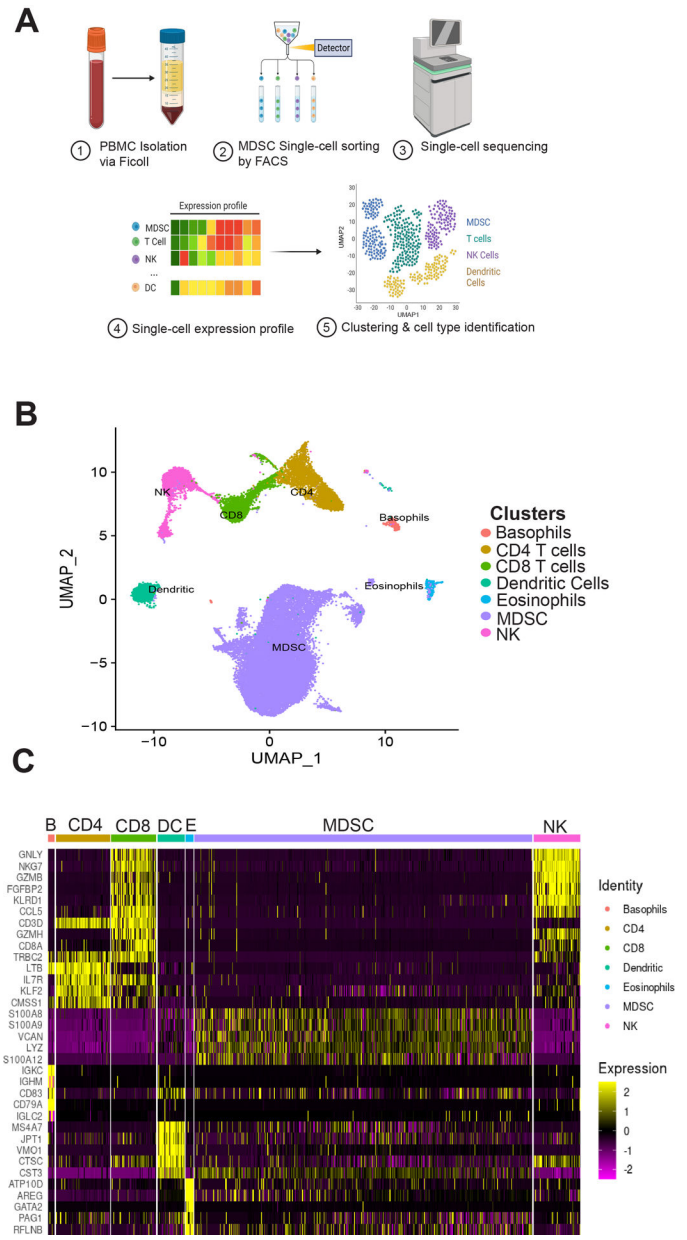

Figure 1. Cell groupings identified by single cell RNA-seq analysis of cancer PBMC enriched for MDSC.

(**A**) Schematic representation of the study workflow. PBMC were isolated from the blood of melanoma (n=3), head & neck (n=1), and breast (n=1) cancer patients. MDSC ($CD11b^{+}$, $CD33^{+}$, $HLA\text{-}DR^{lo/-}$) were isolated using fluorescence-activated cell sorting (FACS) and transcriptome analysis was performed. (**B**) UMAP plot of all samples. (**C**) Heatmap of canonical gene markers used to verify identity of cell clusters (pangloDB).

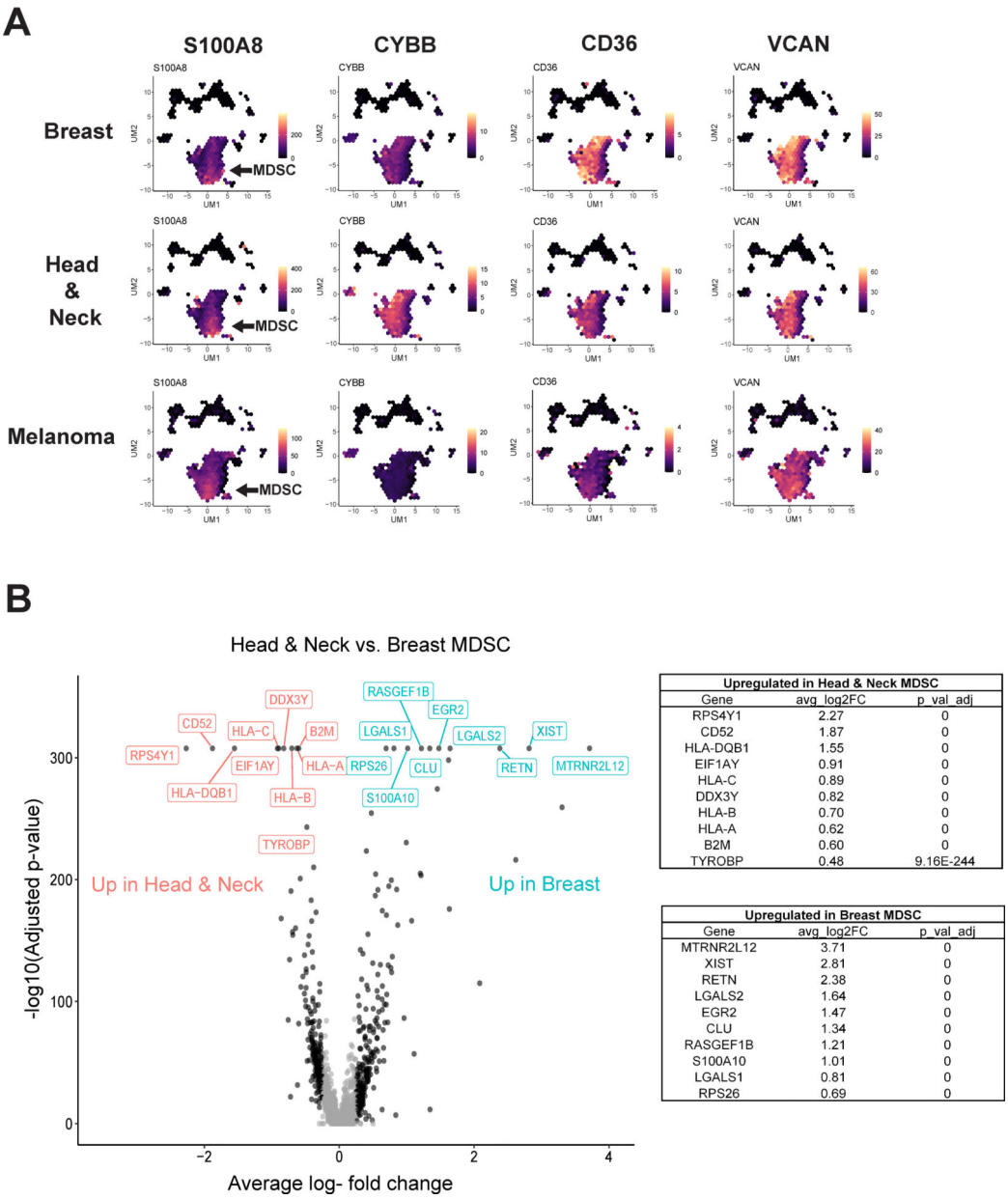

Upregulated in Head & Neck MDSC		
Gene	avg_log2FC	p_val_adj
RPS4Y1	2.27	0
CD52	1.87	0
HLA-DQB1	1.55	0
EIF1AY	0.91	0
HLA-C	0.89	0
DDX3Y	0.82	0
HLA-B	0.70	0
HLA-A	0.62	0
B2M	0.60	0
TYROBP	0.48	9.16E-244

Upregulated in Breast MDSC		
Gene	avg_log2FC	p_val_adj
MTRNR2L12	3.71	0
XIST	2.81	0
RETN	2.38	0
LGALS2	1.64	0
EGR2	1.47	0
CLU	1.34	0
RASGEF1B	1.21	0
S100A10	1.01	0
LGALS1	0.81	0
RPS26	0.69	0

Figure 2. Baseline gene expression of MDSC from different cancer types.

(**A**) UMAP plots of genes expressed by MDSC relative to other cell populations in different cancers (breast, head and neck, melanoma) n=1 each cancer. (**B**) Volcano plot of differentially expressed (DE) genes in breast MDSC relative to head & neck MDSC. Top 10 upregulated genes in MDSC cluster in each cancer type are listed in the table.

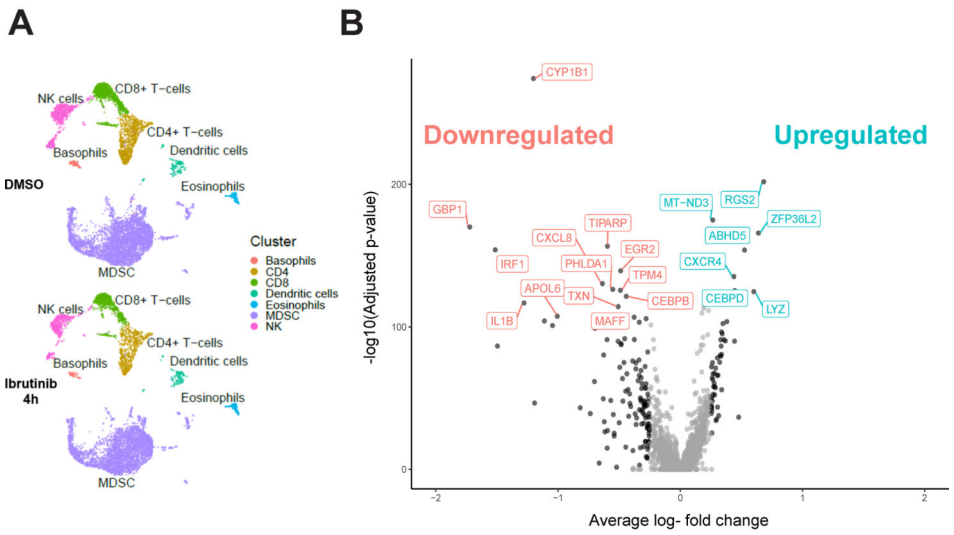

C

Downregulated genes after IBR treatment		
Gene	avg_logFC	p_val_adj
GBP1	-1.72	1.01E-170
IRF1	-1.51	1.15E-154
CXCL10	-1.50	3.08E-87
IL1B	-1.28	1.77E-117
CYP1B1	-1.20	6.26E-275
GBP5	-1.19	3.31E-47
SERPINB2	-1.11	7.21E-105
STAT1	-1.05	1.23E-101
APOL6	-1.01	3.80E-108
GBP2	-0.82	7.02E-44
PLEK	-0.74	8.19E-40
GBP4	-0.70	2.83E-62
JUN	-0.70	9.71E-100
RNF213	-0.66	4.87E-05
CXCL8	-0.64	6.34E-131
IL1RN	-0.63	3.70E-50
CCL3	-0.63	6.05E-81
FABP5	-0.62	4.70E-34
TNFAIP2	-0.62	4.93E-27
BTG2	-0.60	9.82E-92
PARP14	-0.60	1.56E-15
TIPARP	-0.60	3.12E-157
CXCL3	-0.59	7.49E-28
LAP3	-0.57	5.45E-49
PHLDA1	-0.55	4.94E-127
THBS1	-0.55	4.24E-39

Upregulated genes after IBR treatment		
Gene	avg_logFC	p_val_adj
RGS2	0.68	1.90E-202
ZFP36L2	0.64	2.01E-166
LYZ	0.60	1.94E-125
ABHD5	0.53	1.57E-154

Figure 3. In vitro ibrutinib treatment of MDSC from melanoma patients results in significant changes in gene expression.

(**A**) UMAP plots of melanoma MDSC (n=2) treated with control (DMSO) or ibrutinib 5 μM for 4 hours. (**B**) Volcano plot of DE genes in melanoma MDSC after treatment with ibrutinib. (**C**) Table listing upregulated and downregulated genes in MDSC after ibrutinib treatment (0.5 absolute $\log_2$-fold change cutoff).

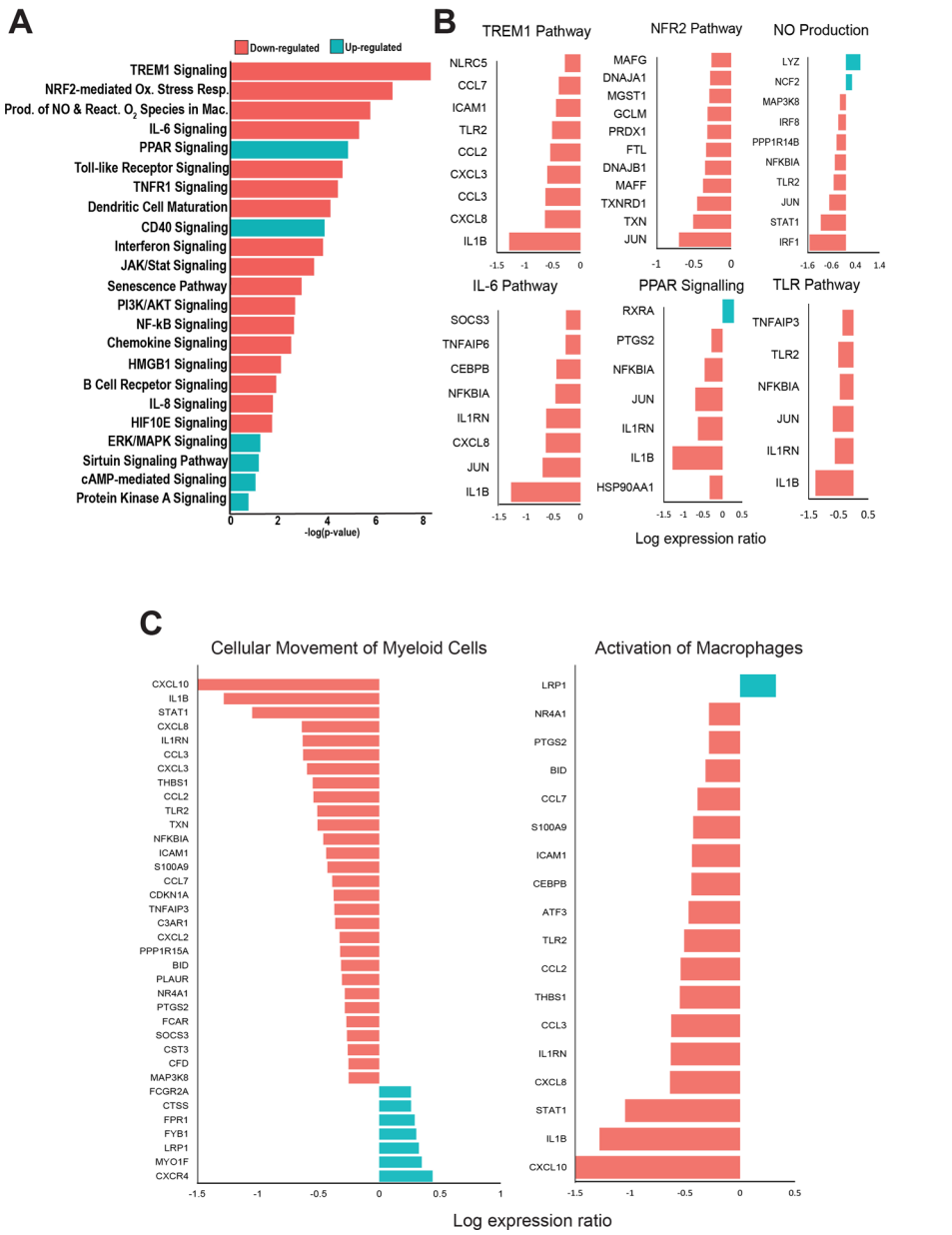

Figure 4. Pathway analysis of gene expression changes in MDSC following BTK inhibition.

Significantly DE genes ($p<0.01$) in the melanoma MDSC cluster after ibrutinib treatment (n=2) were analyzed via Ingenuity Pathway Analysis (IPA). (**A**) Bar chart displaying regulated pathways after ibrutinib treatment. Colors indicate directionality of affected pathway with positive z scores displayed as blue/upregulated and negative z scores displayed as red/downregulated. (**B**) Log expression ratio of individual genes in each pathway after ibrutinib treatment. (**C**) Log expression ratio of genes involved in cellular movement and activation after ibrutinib treatment.

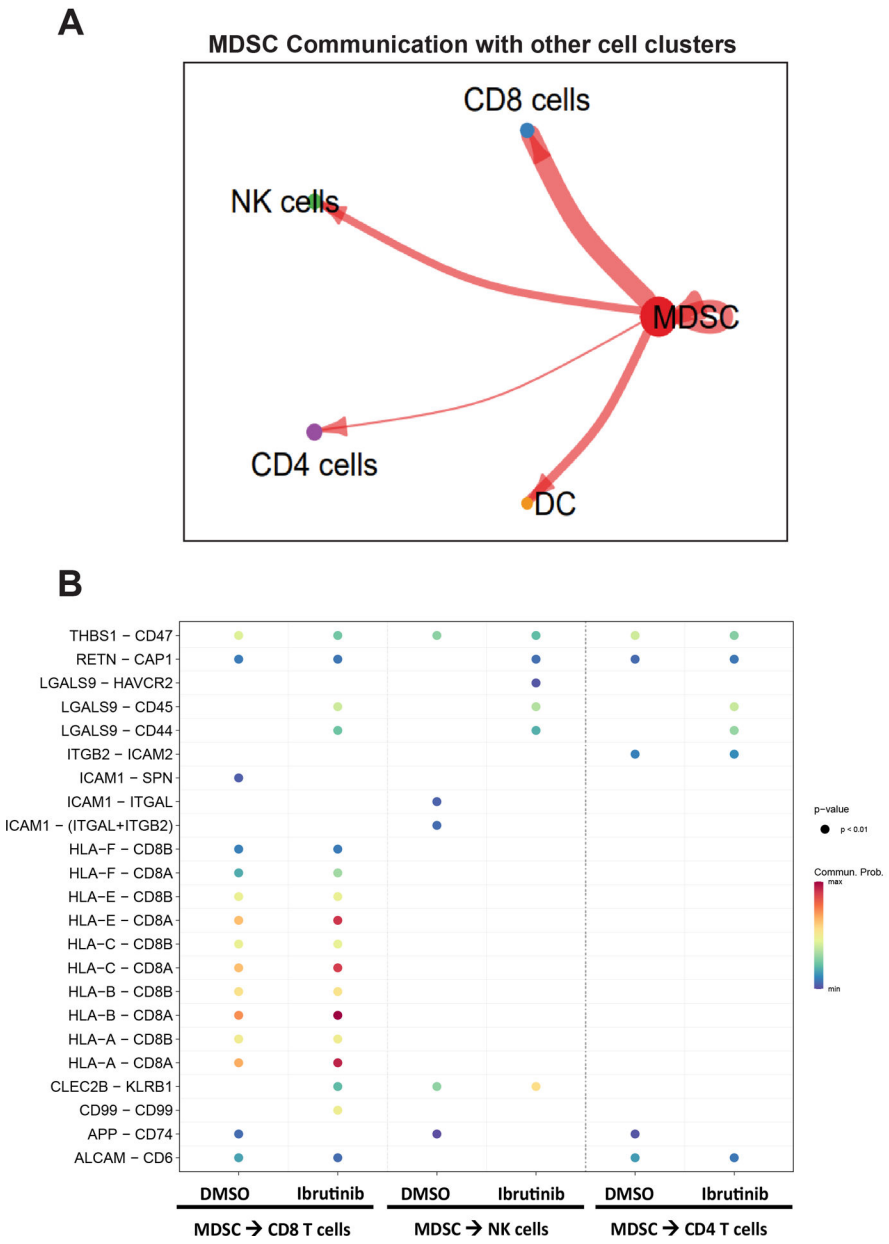

Figure 5. MDSC cell cluster interaction with CD8$^+$ T cells, CD4$^+$ T cells, and NK cells.

(A) Circle plot displaying MDSC cell cluster communication with others cell clusters (CD8$^+$ T cells, CD4$^+$ T cells, NK cells, dendritic cells) from DMSO and ibrutinib treated MDSC. The weight of the arrows indicates a greater number of ligands-receptor pairs. (**B**) Receptor-ligand information flow enrichment of MDSC interaction with each cluster in DMSO treatment and ibrutinib treatment $p<0.01$. The probability of communication is displayed as minimal communication (blue) and maximum communication (red).

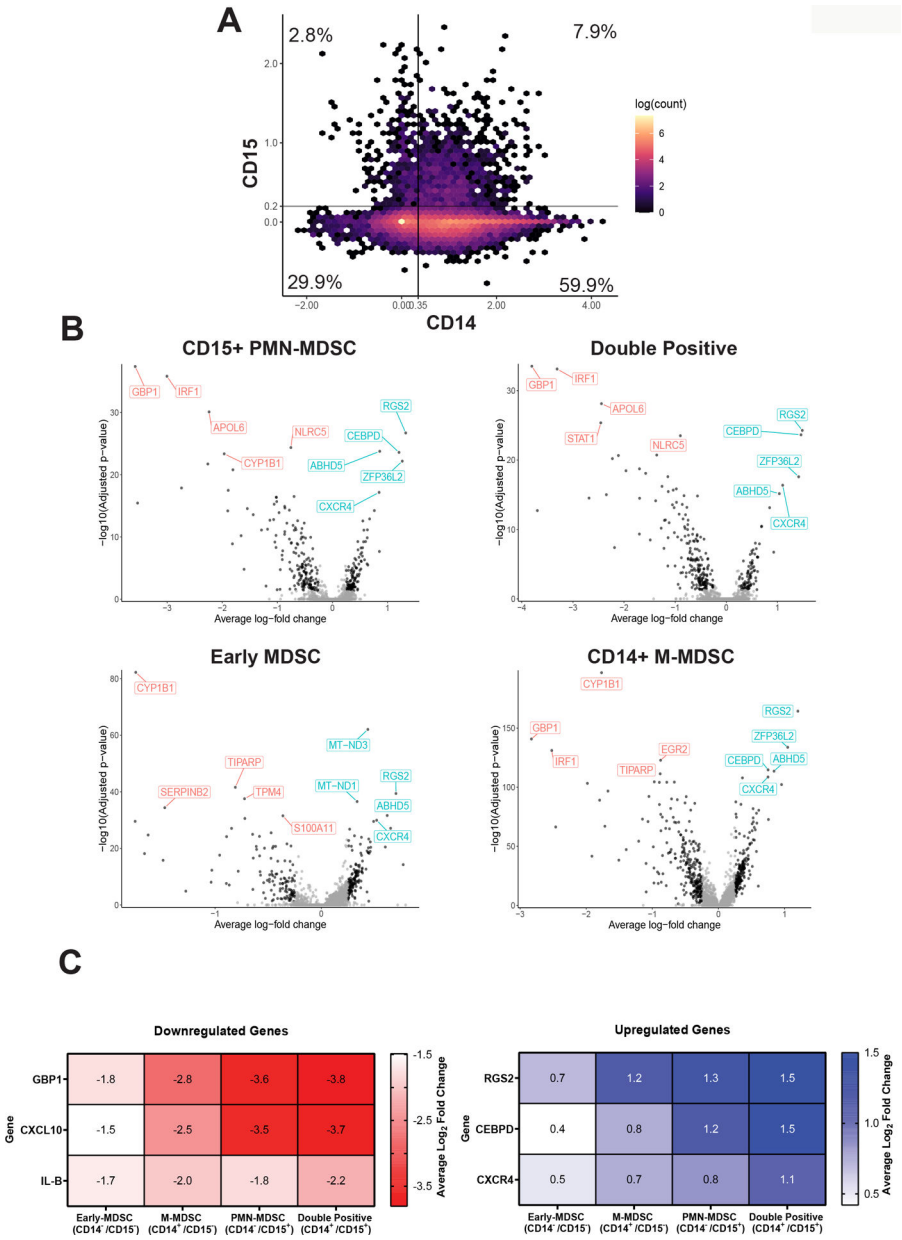

Figure 6. MDSC subset gene expression mirrors total MDSC gene changes after in vitro ibrutinib treatment.

(**A**) Distribution of MDSC subsets in melanoma MDSC. M-MDSC ($CD14^{+}CD15^{-}$, 59.9%), PMN-MDSC ($CD14^{-}CD15^{+}$, 2.8%), double positives ($CD14^{+}CD15^{+}$, 7.9%), and early-MDSC ($CD14^{-}CD15^{-}$, 29.4%). (**B**) Volcano plot of DE genes in melanoma MDSC subsets after treatment with ibrutinib. (**C**) Heatmap of average log_2-fold change of select genes after ibrutinib treatment in MDSC subsets.

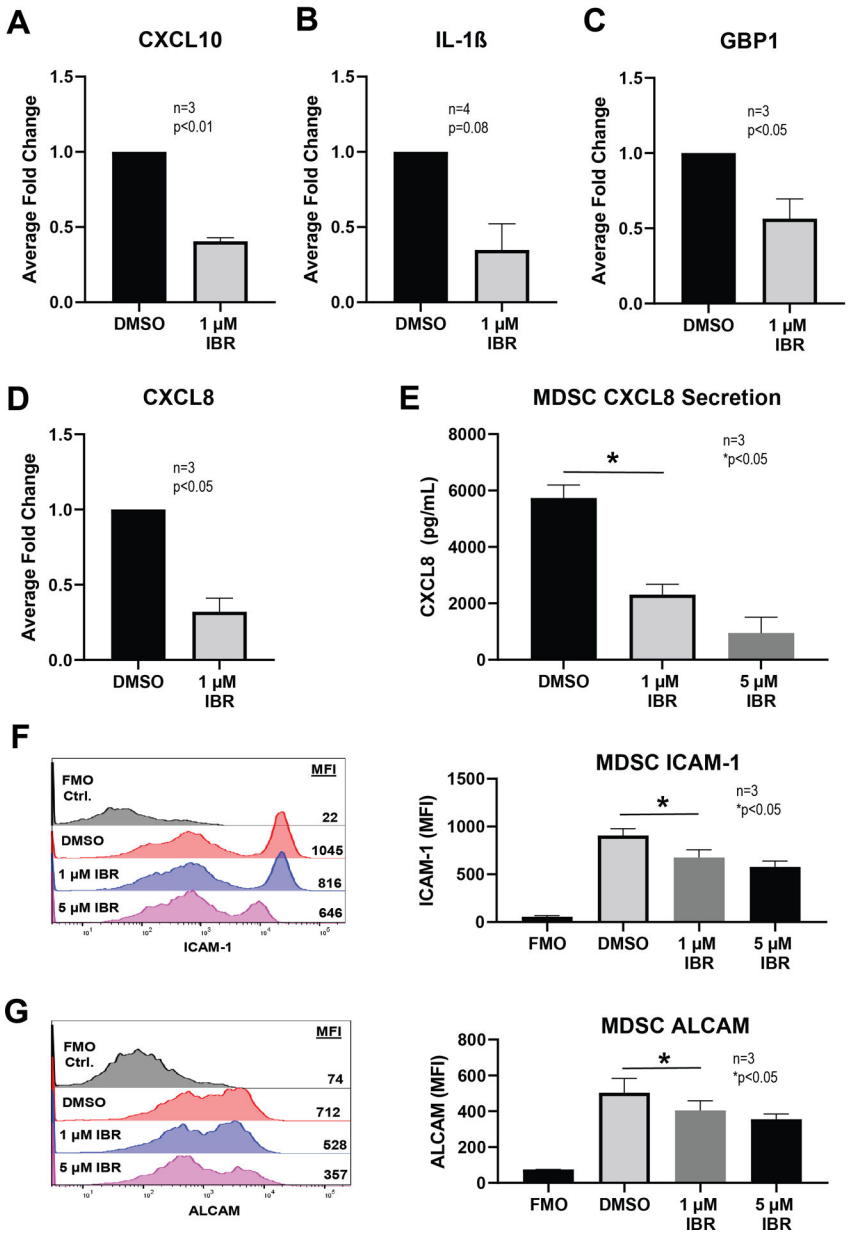

Figure 7. PCR and protein analysis of select genes mirrors single cell analysis gene changes in MDSC after BTK inhibition.

PBMC were isolated from melanoma patients (n=3–4) and purified for MDSC using FACS. MDSC were treated for 6h with 1 μM ibrutinib and RNA was isolated. Gene expression of selected genes was quantified using PCR with *β-actin* as housekeeping gene. (**A**) *CXCL10* (*p<0.01, n=3), (**B**) *IL-1β* (p=0.08, n=4), (**C**) *GBP1* (*p<0.05, n=3), and (**D**) *CXCL8* (*p<0.05, n=3). (**E**) MDSC were treated for 24h with DMSO or ibrutinib (1–5 μM), and CXCL8 was measured in the supernatant via ELISA. **(F-G)** MDSC treated as in E and expression of **(F)** ICAM (*p<0.05 n=3), and **(G)** ALCAM (*p<0.05 n=3) was measured by flow cytometry. Median fluorescence intensity (MFI) for ICAM and ALCAM was calculated and graphed. Representative histograms of the expression of ICAM and ALCAM

by MDSC after treatment. Bar graphs quantifying MFI. (Statistics: Paired students t tests for all comparisons)